IEEE Access
Multidisciplinary | Rapid Review | Open Access Journal

Received October 23, 2018, accepted November 10, 2018, date of publication November 19, 2018,
date of current version December 19, 2018.

Digital Object Identifier 10.1109/ACCESS.2018.2881949

Stochastic Resilient Post-Hurricane Power System Recovery Based on Mobile Emergency Resources and Reconfigurable Networked Microgrids

ABDOLLAH KAVOUSI-FARD, (Member, IEEE), MENGQI WANG, (Member, IEEE), AND WENCONG SU, (Senior Member, IEEE)
ECE Department, University of Michigan-Dearborn, Inskter, MI 80280, USA
Corresponding author: Mengqi Wang (mengqiw@umich.edu)

ABSTRACT This paper develops an effective two-stage stochastic post-hurricane recovery framework to improve networked microgrid resilience using mobile emergency resources (MERs) and a proposed reconfiguration strategy. In the first stage, network reconfiguration actively alters the local power flow path and provides opportunities for restoring critical loads, thus reducing the energy not supplied to electric consumers. The optimal schedule determined in the first stage problem is also used to determine the islanded loads that need MERs for restoration. In the second stage, truck-mounted MERs will deliver power to islanded loads, observing the shortest path and post-hurricane transportation infrastructure constraints. Dijkstra's algorithm is used to produce the shortest path and avoid possible out-of-service roads. In order to model the uncertainties of the problem, a stochastic framework based on unscented transform is employed. The proposed problem is formulated as a two-stage stochastic single-objective optimization problem maximizing system resilience. Simulation results on a test networked microgrid demonstrate the effectiveness and satisfying performance of the proposed model.

INDEX TERMS Stochastic resilient framework, networked microgrids, feeder reconfiguration, mobile emergency resources.

NOMENCLATURE

SETS/INDICES

$\underline{\ }, \overline{\ }$	Minimum, Maximum values
$\Omega^{DL}/lm, mn$	Set/indices of distribution lines
$\Omega^{TL}/lm, mn$	Set/indices of tie lines
$\Omega^{TE}/i, j$	Set/indices of transportation paths (or graph edges)
Ω_k^B/m	Set/index of all buses in kth microgrid
Ω_k^{B*}/m	Set/index of updated buses after removing islanded buses in kth microgrid
$\Omega^{MG}/k, l$	Set/indices of microgrids
Ω_k^{BG}	Set of buses with DG units in kth microgrid
Ω^{BMG}/n	Set/index of buses with MERs
Ω_k^{BS}	Set of buses with energy storage in kth microgrid
Ω^T/t	Set/index of time periods
Ω^S/s	Set/index of initial locations of MERs
Ω^u/u	Set/index of concentration sample points in UT
Ω^{Δ}	Set of transportation line weights
$\Omega^{J/J*}$	Set of temporary/permanent nodes in the transportation system
λ	Index of piecewise linearization segments
pe/te	Symbols showing permanent/temporary status of a node

CONSTANTS

$\underline{C_m^S}, \overline{C_m^S}$	Minimum/maximum allowable stored energy (kWh)
$\underline{CT_m^S}, \underline{DT_m^S}$	Minimum charging/discharging time (hr)
$\overline{I^L}$	Maximum current flow of distribution lines (A)
$\underline{P_m^{Ch}}, \overline{P_m^{Ch}}$	Minimum/maximum charging power (kW)
$\underline{P_m^{Disch}}, \overline{P_m^{Disch}}$	Minimum/maximum discharging power (kW)
$\underline{P_m^G}, \overline{P_m^G}$	Minimum/maximum active power of DG units (kW)

$\underline{P_n^{MER}}, \overline{P_n^{MER}}$	Minimum/maximum active power of MERs (kW)
$\overline{P_l^{MG}}, \overline{Q_l^{MG}}$	Maximum active/reactive power of the microgrid (kW)
$\underline{Q_m^G}, \overline{Q_m^G}$	Minimum/maximum reactive power of DG units (kVar)
$\underline{Q_n^{MER}}, \overline{Q_n^{MER}}$	Minimum/maximum reactive power of MERs (kVar)
R_{mn}, X_{mn}, Z_{mn}	Resistance/reactance/impedance of distribution lines (ohm)
RU_m^G, RD_m^G	Ramp up/down rate of DG units (kW)
T^O	Restoration time period
UT_m^G, DT_m^G	Minimum up/down time of DG units (kW)
$\underline{V}, \overline{V}$	Minimum/maximum voltage magnitude limits (V)
V^{norm}	Nominal voltage of the system (V)
$W_{m,k}$	Weight (significance) of the load on mth bus
δ	Time period (1 hr)
$\eta_m^{Ch}, \eta_m^{Disch}$	Charging/discharging efficiency
ρ_m^G / ρ_n^{MER}	Generation cost of DG/MER unit ($/kW)
Λ	Number of segments of piecewise linear curve
β_u	Weighting factor of sample points in UT
ν	Number of uncertain parameters/variables
μ	Mean value of the uncertain parameter

VARIABLES

$C_{m,k,t}^S$	Energy stored in energy storage units (kWh)
$I_{mn,k,t}^L$	Current flow of distribution lines (A)
$P_{m,k,t}^{Ch}, P_{m,k,t}^{Disch}$	Charging/discharging power (kW)
$P_{m,k,t}^D, Q_{m,k,t}^D$	Active/reactive power demand (kW/kVar)
$P_{mn,k,t}^L, Q_{mn,k,t}^L$	Active/reactive power flow of distribution lines (kW/kVar)
$P_{m,k,t}^G, Q_{m,k,t}^G$	Active/reactive power of DG units (kW/kVar)
$P_{l,k,t}^M, Q_{l,k,t}^M$	Active/reactive power of utility grid (kW/kVar)
$P_{n,k,t}^{MER}, Q_{n,k,t}^{MER}$	Active/reactive power of MERs (kW/kVar)
$T_{m,k,t}^{Ch}, T_{m,k,t}^{Disch}$	Number of successive charging/discharging hours (hr)
$T_{m,k,t}^{G-on}, T_{m,k,t}^{G-off}$	Number of successive on/off hours for DGs (hr)
T_{CL}	Service time of the load in post-hurricane restoration (hr)
$V_{m,k,t}$	Voltage magnitude of buses (V)
$w_{mn,k,t}^L$	Distribution line status
$x_{m,k,t}^G$	Commitment state of DG units
$x_{n,k,t}^{MER}$	Binary variable showing presence/lack off MERs in a location
$\bar{x}_{k,t}^{MER}$	Maximum number of truck-mounted MERs available in a microgrid
$y_{m,k,t}^{Ch}, y_{m,k,t}^{Disch}$	Charging/discharging state of energy storage units
$\Delta V_{mn,k,t}$	Variable needed to apply KVL to distribution lines
$\theta_{mn,t}^L$	Fictitious current flow of distribution lines
$\theta_{m,k,t}^M$	Fictitious current flow of utility grid
$\theta_{m,k,t}^D$	Fictitious current flow demand

I. INTRODUCTION

Extreme weather disasters, particularly hurricanes, can cause severe issues in distribution systems, resulting in long-term load outages, power quality deterioration and economic losses [1]. In the United States, weather disasters have caused over 80% of long-term power outages involving more than 50,000 electric consumers [2]. In the first half of 2016, eight weather disasters (including floods, storms and hurricanes) in the United States caused financial damages with losses of over $1 billion each [3]. In August 2017, Hurricane Harvey damages cost up to $180 billion and caused long-term electricity outages that lasted up to several weeks in some towns. Other recent hurricanes, such as Hurricane Ike, Hurricane Irene, Superstorm Sandy, and Typhoon Soudelor, which struck the United States and China in 2008, 2011, 2012, and 2015, respectively, caused severe damage to power grid infrastructures, which led to widespread power outages [4]–[6]. These events led to the concept of resiliency in electrical engineering studies, meaning the ability of a grid to resist and recover from severe disturbances. By this definition, a resilient system is one that maintains an active awareness of surrounding threats and reacts to those threats in a manner that returns the system to operational normalcy in finite time [7].

In recent years, several research studies have been implemented to analyze system resiliency and suggest a couple of resilience-based models and reinforcement strategies [8]–[10]. In [11], distributed generations (DGs), along with the microgrid model, are employed for restoring the loads on buses adjacent to DGs. The concept of continuous operating time is proposed to settle microgrid availability for load restoration and to evaluate service time [12]. In [13], the microgrid idea is used to reduce the congestion level of feeders in areas with power outages, releasing their capacity to enable higher power supply to the affected loads. In [14], a mixed integer nonlinear programming framework is proposed to make use of microgrids for restoring the electric grid. A distribution operational algorithm is developed in [15] to restore critical loads by formation of multiple microgrids after a weather disaster. Local communications are used for global information discovery and coordinating DGs. In [16], a self-healing strategy is presented to schedule dispatchable DGs during both normal and faulty conditions. In the normal

operation, the objective function maximizes grid revenue, and in the faulty condition, the target is to maximize the load supplement continuously. The feasibility of employing microgrids as resiliency sources, and the possible advantages and technical challenges of doing so, are addressed in [17]. The above research works have only focused on the electrical grid and have ignored damages involved in other critical infrastructures. It is clear, however, that a practical resilient framework needs to address damages to other infrastructures to maximize operational capacity. In [18] and [19], the interdependency of critical infrastructures in natural disasters is assessed during electric load restoration. It is shown that as part of the feasible planning and operation of power systems, the physical constraints due to the disaster need to be taken into account.

As is gleaned from the above survey of existing work, the high complexity, unpredictability and versatile nature of natural disasters, such as hurricanes, have created largely diverse research activities. From the time domain aspect, and to clearly determine the scope of this paper, the response timeline of the electric grid in the case of a hurricane is divided into three groups: pre-hurricane, hurricane-time and post-hurricane. Fig. 1 shows a list of strategies available for improving system resilience before and after a hurricane. This paper focuses on the post-hurricane activities, which aim to recover the loads and increase system resiliency. In post-hurricane literature, the main focus has been on restoring the power supply to the electrical loads using DGs and microgrids. Optimal switching is another solution, which has been investigated by some research as a practical and fast restoration tool [20], [21]. In [22], the role of switching, microgrids and DGs in load restoration is assessed based on automation technology. While each of these works has investigated a critical part of system resiliency, none of them has considered the significant role of mobile emergency resources (MERs) in fast load recovery. To the best of the authors' knowledge, the only work that has addressed the role of MERs in achieving system resiliency is [23]. In [23], truck-mounted MERs are pre-positioned at the appropriate locations before a hurricane and then are dispatched as DGs to restore electrical loads during the real-time allocation that occurs after the hurricane. The microgrid formation concept is also used to divide the system into several microgrids with the capability of an islanding mode. While this work provides

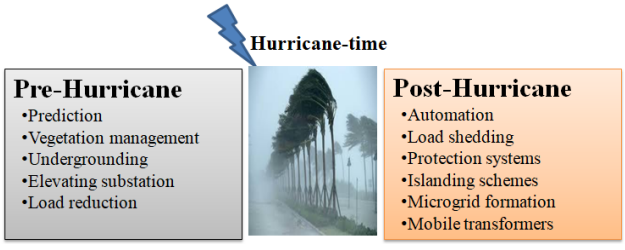

FIGURE 1. Some of the electric grid strategies for use before and after a hurricane [12].

valuable results regarding the effect of MERs on power system resiliency, it has not considered the interdependency of the critical transportation infrastructure involved in restoring the electrical loads. This interdependency is a significant issue in the area of power system restoration, especially in the post-hurricane scenario, when some routes may be damaged and unusable.

As can be inferred from Fig. 1, there are several methods presented for power system restoration after a severe event/fault. Automation, load shedding, special protection schemes, fast islanding detection schemes and mobile transformers are among these methods [11]. To this end, a microgrid formation mechanism to restore critical loads after a major fault is a widely accepted concept by researchers for improving power quality after natural disasters [15]. In fact, any automated distribution system equipped with remotely controlled switches and DGs is capable of microgrid formation after a natural disaster. Given this fact, this paper mainly focuses on automated electric grids that are equipped with remotely controlled switches for reconfiguration. To enhance the problem one more step, we have considered the potential of dividing an automated grid into several microgrids (called networked-microgrids), which can decide to either operate in islanded mode or connected mode according to the situation. Certainly, in the normal operation, economic preferences, such as optimizing the total cost, are considered; however, in an abnormal situation, such as after a hurricane, the main priority is given to load supplement, which is presented in the form of the resilient objective function shown in (3). It is clear that in a distribution system without automation capability, other resilient reinforcement solutions may apply. According to these discussions, this paper focuses on the resilient performance of networked microgrids based on MERs and remotely controlled switches, which are used as effective practical leverages for load restoration in the post-hurricane period. In networked microgrids, the concept of cooperative power scheduling commitment can help provide resiliency in an emergency situation. Thus, a sufficient stochastic two-stage operation and management framework is developed to increase networked microgrid resiliency performance function by maximizing the amount of critical load restored and minimizing the restoration time. Due to the instant operation and control capability of remotely controlled switches, a reconfiguration technique is used in the first stage to alter the network topology and provide replacement paths for energizing the affected loads. By appropriate formulation in the first stage, buses that still experience loss or shortage of power after the reconfiguration are determined and considered as candidates for power delivery by MERS in the next stage. In the second stage, truck-mounted MERs deliver power to the islanded buses, observing the shortest path target and possible post-hurricane transportation infrastructure limitations. To this end, Dijkstra's algorithm is used to produce the shortest path while avoiding damaged roads. In addition, an effective stochastic framework based on unscented transform (UT)

is proposed to model the uncertainties associated with the traveling time of truck-mounted MERs to the affected buses, as well as the active and reactive load values. UT is a newly introduced superposition and has shown great performance in nonlinear transformations, state estimators and uncertainty modeling in the correlated environments [21]. In summary, the main contributions of this work are:

- Developing an effective stochastic two-stage post-hurricane resilient framework for networked microgrids.
- Proposing an accurate linear power flow for reconfigurable networked microgrids with islanding capability.
- Developing a sufficient stochastic framework based on UT for modeling the uncertainties of the problem of post-hurricane load restoration, including truck-mounted MERs' travel time and active/reactive load demand.
- Leveraging truck-mounted MERs in conjunction with reconfiguration to minimize electric consumers' outage time duration.

The rest of this paper is organized as follows. Section II explains the problem formulation and component modeling and elaborates on the objective and relevant constraints. Section III describes Dijkstra's algorithm as the shortest-path algorithm. Section IV describes the stochastic framework based on UT. Section V presents illustrative scenarios to show the proposed model applied to a test networked microgrid. Discussions on the results and features of the proposed model are provided in Sections VI and VII.

II. PROBLEM FORMULATION AND COMPONENT MODELING

This section develops the problem formulation, including the objective function and constraints, and models the multi-microgrid distribution network and its components to allow the use of these models in the proposed resilient optimization problem.

A. OBJECTIVE FUNCTION

The objective function maximizes system resilience in the post-hurricane restoration stage, i.e., the time period for restoring loads using either reconfiguration or MERs. In order to evaluate the system resilience objective function, Fig. 2 shows an electric system resilience curve for a typical extreme event.

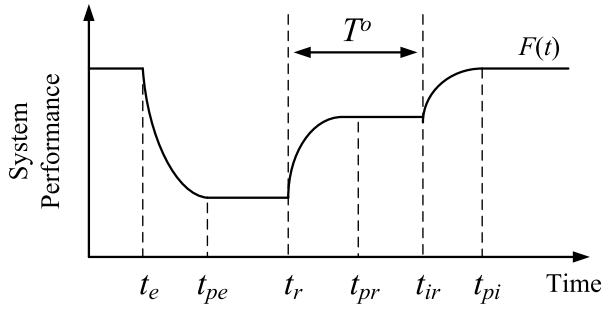

FIGURE 2. Electric system resilience curve for a typical extreme event [6].

In Fig. 2, $F(t)$ represents the system performance function, including the hurricane event progress state $[t_e, t_{pe}]$, post-event degraded state $[t_{pe}, t_r]$, restoring state $[t_r, t_{pr}]$, post-restoration state $[t_{pr}, t_{ir}]$, and infrastructure recovery $[t_{ir}, t_{pr}]$ [6]. Considering satellite big data provided before a hurricane [24]–[26], MERs are allocated to the most appropriate places close enough to the hurricane path for fast delivery to damaged areas. In the post-hurricane period, the main time for focusing on improving system resilience is in the range $[t_r, t_{ir}]$, i.e., the restoration and post-restoration states. During this time period, post-hurricane restoration strategies should be employed to supply critical loads. After the hurricane and based on the prediction methods and the distribution system crew's experience, the length of the outage time T^0 is estimated. Therefore, the restoration strategies are implemented during the time $[t_r, t_r+T^O]$, and after t_r+T^O, normal utility power activities are resumed to serve the loads.

According to Fig. 2, system resilience in the post-hurricane restoration stage, i.e., the time period concerned with reconfiguration and MER allocation, is evaluated by the integral of the performance function over the time period minus the generators' cost [6]:

$$R = \gamma \times \int_{t_r}^{t_r+T^0} F(t)dt - G \tag{1}$$

In the above equation, R represents the resilience index in the integral bandwidth of $[t_r, t_r + T^0]$. Therefore, increasing R, either by maximizing $F(t)$ or minimizing G, will enhance system resilience. The parameter γ is used to convert energy into its equivalent money value. The system performance $F(t)$ is then evaluated as the total electrical energy supplied to consumers based on their weighting priority [6]:

$$F(t) = \sum_{\forall k \in \Omega^{MG}} \sum_{\forall m \in \Omega^B} W_{m,k} P^D_{m,k,t}, \quad t \in \left[t_r, t_r + T^0\right] \tag{2}$$

Considering T_{CL} as the service time of the load during post-hurricane restoration, the R formulation in (1) is updated as follows:

$$\begin{aligned} R &= \gamma \times \int_{t_r}^{t_r+T^0} \left(\sum_{\forall m \in \Omega^B} W_{m,k} P^D_{m,k,t} \right) dt - G \quad \forall k \in \Omega^{MG} \\ &= \gamma \times \sum_{\forall m \in \Omega^B} W_{m,k} \int_{t_r}^{t_r+T^0} P^D_{m,k,t} dt - G \\ &= \gamma \times \sum_{\forall m \in \Omega^B} W_{m,k} \int_{t_r}^{t_r+T^{CL}} P^D_{m,k,t} dt - G \\ &= \gamma \times \sum_{\forall m \in \Omega^B} W_{m,k} P^D_{m,k} T^{CL}_{m,k} - G \end{aligned} \tag{3}$$

The variable T^{CL} will be determined from the second stage based on either reconfiguration or Dijkstra's algorithm (travel

time of MERs to the loads). Term G in (3) specifies the power generation cost to make it possible to restore the multi-microgrid system with the fewest number of DGs and MERs:

$$G=\sum_{t\in\Omega^T}\left(\sum_{k\in\Omega^{MG}}\left(\sum_{m\in\Omega^{BG}}\rho_m^G P_{m,t}^G+\sum_{n\in\Omega^{BMG}}\rho_n^{MER}P_{n,t}^{MER}\right)\right)\delta \tag{4}$$

In the proposed model, faulty components that cannot be restored are removed from the rest of the electric grid in successive steps with short time delays. Remotely controlled switches (RCSs) with a fast control mechanism in the smart grids make it is possible to ignore small delays during the fault clearing process, though these small delays are of high significance in the transient stability analysis of the power system, where the active and reactive power control is made by the automatic generation control (AGC) system. Therefore, it is clear that these short delays cannot significantly affect the objective function value in our case. In the remainder of this section, first a mixed-integer nonlinear programming (MINLP) model reflecting all the necessary operational characteristics of the grid is proposed. In order to obtain a more well-mannered problem formulation, the proposed MINLP model is then converted into a mixed-integer linear programming (MILP) model using a highly accurate linearization method.

B. COMPONENT MODELING

Microgrid components are modeled using (5)-(10) for dispatchable DGs and (11)-(17) for distributed energy sources (DESs).

Equations (5)-(6) show the active and reactive power capacity limitations of a DG:

$$\underline{P_{m,k}^G}x_{m,k,t}^G\le P_{m,k,t}^G\le\overline{P_{m,k}^G}x_{m,k,t}^G \quad \forall k\in\Omega^{MG},\ \forall m\in\Omega_k^{BG},\ \forall t\in\Omega^T \tag{5}$$

$$\underline{Q_{m,k}^G}x_{m,k,t}^G\le Q_{m,k,t}^G\le\overline{Q_{m,k}^G}x_{m,k,t}^G \quad \forall k\in\Omega^{MG},\ \forall m\in\Omega_k^{BG},\ \forall t\in\Omega^T \tag{6}$$

Equations (7)-(8) show the ramp up and ramp down rate limits:

$$P_{m,k,t}^G-P_{m,k,t-1}^G\le RU_{m,k}^G \quad \forall k\in\Omega^{MG},\ \forall m\in\Omega_k^{BG},\ \forall t\in\Omega^T \tag{7}$$

$$P_{m,k,t-1}^G-P_{m,k,t}^G\le RD_{m,k}^G \quad \forall k\in\Omega^{MG},\ \forall m\in\Omega_k^{BG},\ \forall t\in\Omega^T \tag{8}$$

Equations (9)-(10) represent the minimum up and down time limits:

$$T_{m,k,t}^{G-on}\ge UT_{m,k}^G\left(x_{m,k,t}^G-x_{m,k,t-1}^G\right) \quad \forall k\in\Omega^{MG},\ \forall m\in\Omega_k^{BG},\ \forall t\in\Omega^T \tag{9}$$

$$T_{m,k,t}^{G-off}\ge DT_{m,k}^G\left(x_{m,k,t-1}^G-x_{m,k,t}^G\right) \quad \forall k\in\Omega^{MG},\ \forall m\in\Omega_k^{BG},\ \forall t\in\Omega^T \tag{10}$$

Constraints (11)-(12) ensure the limiting bounds on the MERs:

$$\underline{P_{n,k}^{MER}}x_{n,k,t}^{MER}\le P_{n,k,t}^{MER}\le\overline{P_{n,k}^{MER}}x_{n,k,t}^{MER} \quad \forall k\in\Omega^{MG},\ \forall n\in\Omega_k^{MER},\ \forall t\in\Omega^T \tag{11}$$

$$\underline{Q_{n,k}^{MER}}x_{n,k,t}^{MER}\le Q_{n,k,t}^{MER}\le\overline{Q_{n,k}^{MER}}x_{n,k,t}^{MER} \quad \forall k\in\Omega^{MG},\ \forall n\in\Omega_k^{MER},\ \forall t\in\Omega^T \tag{12}$$

For DESs, (13)-(14) show the minimum and maximum charging and discharging limits:

$$\underline{P_{m,k}^{Ch}}y_{m,k,t}^{Ch}\le P_{m,k,t}^{Ch}\le\overline{P_{m,k}^{Ch}}y_{m,k,t}^{Ch} \quad \forall k\in\Omega^{MG},\ \forall m\in\Omega_k^{BS},\ \forall t\in\Omega^T \tag{13}$$

$$\underline{P_{m,k}^{Disch}}y_{m,k,t}^{Disch}\le P_{m,k,t}^{Disch}\le\overline{P_{m,k}^{Disch}}y_{m,k,t}^{Disch} \quad \forall k\in\Omega^{MG},\ \forall m\in\Omega_k^{BS},\ \forall t\in\Omega^T \tag{14}$$

Constraints (15)-(16) present the available energy limit:

$$C_{m,k,t}^S=C_{m,k,t-1}^S-P_{m,k,t}^{Disch}\delta\Big/\eta_{m,k}^{Disch}+P_{m,k,t}^{Ch}\delta\eta_{m,k}^{Ch} \quad \forall k\in\Omega^{MG},\ \forall m\in\Omega_k^{BS},\ \forall t\in\Omega^T \tag{15}$$

$$\underline{C_{m,k}^S}\le C_{m,k,t}^S\le\overline{C_{m,k}^S} \quad \forall k\in\Omega^{MG},\ \forall m\in\Omega_k^{BS},\ \forall t\in\Omega^T \tag{16}$$

Constraints (17)-(18) show the minimum charging and discharging time limits:

$$T_{m,k,t}^{Ch}\ge CT_{m,k}^S\left(y_{m,k,t}^{Ch}-y_{m,k,t-1}^{Ch}\right) \quad \forall k\in\Omega^{MG},\ \forall m\in\Omega_k^{BS},\ \forall t\in\Omega^T \tag{17}$$

$$T_{m,k,t}^{Disch}\ge DT_{m,k}^S\left(y_{m,k,t}^{Disch}-y_{m,k,t-1}^{Disch}\right) \quad \forall k\in\Omega^{MG},\ \forall m\in\Omega_k^{BS},\ \forall t\in\Omega^T \tag{18}$$

Constraint (19) states the operation mode and (20) shows the maximum number of truck-mounted MERs available in a microgrid to provide fast power delivery.

$$y_{m,k,t}^{Ch}+y_{m,k,t}^{Disch}\le 1 \quad \forall k\in\Omega^{MG},\ \forall m\in\Omega_k^{BS},\ \forall t\in\Omega^T \tag{19}$$

$$\sum_n x_{n,k,t}^{MER}\le\bar{x}_{k,t}^{MER} \quad \forall k\in\Omega^{MG},\ \forall t\in\Omega^T \tag{20}$$

In this study, the scheduling interval is assumed to be an hour to model these constraints (t-(t-1) $=\delta=$ 1h). Shorter time intervals can be evaluated in the same manner.

C. MICROGRID DISTRIBUTION NETWORK MODELING

In this part, a linear steady-state model is proposed for the distribution network. The proposed model incorporates the power flow equations for modeling the active and reactive loads, considers switching capability for changing the network topology and determines islanded buses along with the amount of power required to restore them.

As mentioned in the introduction, reconfiguration is used as an active tool for improving system resiliency. The basic architecture for a reconfiguration strategy requires three main

components [5]: 1) devices to be controlled, 2) a communication system, and 3) a central control (CC). The control devices can generally be either manual switches or RCSs that facilitate the change of the network topology. The communication system has the task of transferring data from different parts of the network, such as the measuring devices, protective devices, and the actuators, to the CC. In the case of RCSs, there is no need for any crew member, thus they are appropriate for fast restoration [5]. In other words, it is RCSs that make it possible to isolate a faulty component, either a feeder or bus, in a system. Therefore, there is no need for any further modification/amending of the protection scheme after its initial design.

Eqs. (21)-(29) model the AC power flow in a microgrid based on a set of recursive equations, as demonstrated in Fig. 3. In these formulations, MERs' locations and required capacities are determined, which will be used further in stage 2 for power delivery by truck-mounted MERs. Eqs. (21)-(22) acquire the active and reactive power balances at each system bus, incorporating DGs, DESs, MERs and loads.

$$\begin{aligned}&\sum_{lm\in(\Omega^{DL}\cup\Omega^{TL})}\left[P^{L}_{lm,k,t}-R_{lm,k}\left(I^{L}_{lm,k,t}\right)^{2}\right]\\&\quad-\sum_{mn\in(\Omega^{DL}\cup\Omega^{TL})}P^{L}_{mn,k,t}+P^{G}_{m,k,t}+P^{MER}_{n,k,t}\\&\quad-P^{Ch}_{m,k,t}+P^{Disch}_{m,k,t}+P^{M}_{m,k,t}\\&=P^{D}_{m,k,t}\forall k\in\Omega^{MG},\quad\forall m\in\Omega^{B}_{k},\ \forall n\in\Omega^{MER}_{k},\ \forall t\in\Omega^{T}\end{aligned}\tag{21}$$

$$\begin{aligned}&\sum_{lm\in(\Omega^{DL}\cup\Omega^{TL})}\left[Q^{L}_{lm,k,t}-X_{lm,k}\left(I^{L}_{lm,k,t}\right)^{2}\right]\\&\quad-\sum_{mn\in(\Omega^{DL}\cup\Omega^{TL})}Q^{L}_{mn,k,t}+Q^{G}_{m,k,t}+Q^{MER}_{n,k,t}+Q^{M}_{m,k,t}\\&=Q^{D}_{m,k,t}\\&\quad\forall k\in\Omega^{MG},\quad\forall m\in\Omega^{B}_{k},\ \forall n\in\Omega^{MER}_{k},\ \forall t\in\Omega^{T}\end{aligned}\tag{22}$$

Here, the symbol $P^{M}_{m,k,t}/Q^{M}_{m,k,t}$ represents the amount of active/reactive power transferred between the k^{th} microgrid and the utility.

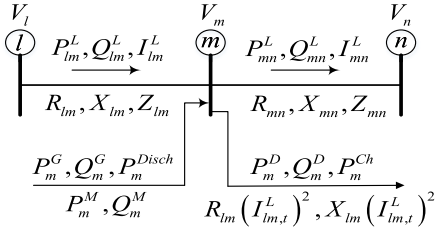

FIGURE 3. Illustration of a radial distribution network.

Eqs. (23)-(24) show Kirchhoff's voltage law (KVL) as it relates to each distribution line. Here, $\Delta V_{mn,k,t}$ is an auxiliary variable that receives a value of zero if line mn is switched on in microgrid k at time period t; otherwise it will have a positive/negative value in proportion to the difference between the voltages of the sending and receiving buses of line mn.

$$\begin{aligned}&\left(V_{m,k,t}\right)^{2}-\left(V_{n,k,t}\right)^{2}\\&=2\left(R_{mn,k}P^{L}_{mn,k,t}+X_{mn,k}Q^{L}_{mn,k,t}\right)\\&\quad-\left(Z_{mn,k}\right)^{2}\left(I^{L}_{mn,k,t}\right)^{2}+\Delta V_{mn,k,t}\quad\forall mn\in\left(\Omega^{DL}\cup\Omega^{TL}\right),\\&\quad\forall k\in\Omega^{MG},\quad\forall t\in\Omega^{T}\end{aligned}\tag{23}$$

$$\begin{aligned}&\left(V_{m,k,t}\right)^{2}\left(I^{L}_{mn,k,t}\right)^{2}\\&=\left(P^{L}_{mn,k,t}\right)^{2}+\left(Q^{L}_{mn,k,t}\right)^{2}\quad\forall mn\in\left(\Omega^{DL}\cup\Omega^{TL}\right),\\&\quad\forall k\in\Omega^{MG},\quad\forall t\in\Omega^{T}\end{aligned}\tag{24}$$

Eq. (25) determines the acceptable range of bus voltage magnitudes.

$$\underline{V}\le V_{m,k,t}\le\overline{V}\quad\forall k\in\Omega^{MG},\ \forall m\in\Omega^{B}_{k},\ \forall t\in\Omega^{T}\tag{25}$$

Eq. (26) is the feeder maximum current flow capacity. It also checks the current of an out of service line to see if it is zero. In (26), the binary variable $w^{L}_{mn,k,t}$ equals one only if the corresponding distribution line is working properly; otherwise it will be equal to zero.

$$0\le I^{L}_{mn,k,t}\le\overline{I^{L}}w^{L}_{mn,k,t}\ \forall k\in\Omega^{MG},\ \forall mn\in\Omega^{DL},\ \forall t\in\Omega^{T}\tag{26}$$

$$0\le I^{L}_{mn,k,t}\le\overline{I^{L}}\ \forall k\in\Omega^{MG},\ \forall mn\in\Omega^{TL},\ \forall t\in\Omega^{T}\tag{27}$$

Eq. (28) sets appropriate bounds on variable $\Delta V_{mn,k,t}$.

$$\begin{aligned}\left|\Delta V_{mn,k,t}\right|\le\left(\overline{V}-\underline{V}\right)\left(1-w^{L}_{mn,k,t}\right)\quad\forall k\in\Omega^{MG},\\\forall mn\in\left(\Omega^{DL}\cup\Omega^{TL}\right),\quad\forall t\in\Omega^{T}\end{aligned}\tag{28}$$

Eqs. (29)-(30) guarantee that the power exchange with the utility grid is limited by the flow limits of the line connecting the microgrid to the utility grid.

$$-\overline{P^{M}_{m,k}}\le P^{M}_{m,k,t}\le\overline{P^{M}_{m,k}}\quad\forall k\in\Omega^{MG},\ \forall m\in\Omega^{B}_{k},\ \forall t\in\Omega^{T}\tag{29}$$

$$-\overline{Q^{M}_{m,k}}\le Q^{M}_{m,k,t}\le\overline{Q^{M}_{m,k}}\quad\forall k\in\Omega^{MG},\ \forall m\in\Omega^{B}_{k},\ \forall t\in\Omega^{T}\tag{30}$$

The radiality constraint is a valid constraint in the optimal operation of a distribution power system. Nevertheless, in an extreme operation mode (after a hurricane), it is quite possible that some damaged buses cannot be restored and will remain islanded. In such a case, which did occur in our problem, maintaining network radiality in the traditional way will force the grid to connect the healthy components to the damaged components and thus put the system in an unstable mode. To deal with this situation, the set of buses in each MG should be updated in each iteration (here, by iteration we mean a single application of any resiliency reinforcement strategy to the system) such that only buses that can escape from being left islanded are included in the set. These buses can

be considered in the reconfiguration process and will obey the radiality constraint. In other words, if a load at bus m can be energized by a microgrid k, it is added to the relevant bus set in the MG, i.e. Ω_k^B. It is clear that any bus with a healthy connecting line through a tie or sectionalizing switch has the potential to be recovered during the reconfiguration process; however, buses with permanent line faults may stay islanded without being connected to any microgrid. Such buses have lost their connection with adjacent buses due to permanent tie and sectionalizing switch failure. These buses should be removed from the set of buses in the relevant MG to avoid any problems for the network radiality constraint. This can be achieved by finding the disconnected nodes of an undirected graph representing the MG system topology and removing the nodes and edges of buses with neither a healthy tie nor sectionalizing connection. Therefore, the updated set of buses, Ω_k^{B*}, which will meet the radiality constraint in each MG k, is as follows:

$$\Omega_k^{B*} = \{m | \exists lm \in \Omega^{TL} OR \exists lm \in \Omega^{DL}\}; \quad \forall k \in \Omega^{MG}, \ \forall t \in \Omega^T \tag{31}$$

Having updated the set of buses, the radiality constraint is satisfied as follows:

$$\sum_{lm \in (\Omega^{DL} \cup \Omega^{TL})} w_{lm,k,t}^L = 1 \quad \forall k \in \Omega^{MG}, \ \forall m \in \Omega_k^{B*}, \ \forall t \in \Omega^T \tag{32}$$

$$\sum_{lm \in \Omega^L} \theta_{lm,k,t}^L - \sum_{mn \in \Omega^L} \theta_{mn,k,t}^L + \theta_{m,k,t}^M = \theta_{m,k,t}^D \quad \forall m \in \Omega^{B*}, \ \forall k \in \Omega^{MG}, \ \forall t \in \Omega^T \tag{33}$$

$$0 \le \theta_{mn,k,t}^L \le \left|\Omega^N\right| w_{mn,k,t}^L \quad \forall k \in \Omega^{MG}, \ \forall mn \in \Omega^{DL}, \ \forall t \in \Omega^T \tag{34}$$

$$0 \le \theta_{mn,k,t}^L \le \left|\Omega^N\right| \quad \forall k \in \Omega^{MG}, \ \forall mn \in \Omega^{TL}, \ \forall t \in \Omega^T \tag{35}$$

$$0 \le \theta_{m,k,t}^M \le \left|\Omega^N\right| \quad \forall k \in \Omega^{MG}, \ \forall m \in \Omega^{B*}, \ \forall t \in \Omega^T \tag{36}$$

$$\theta_{m,k,t}^D = \begin{cases} 1 & \forall m \in \Omega^{B*}, \ \forall k \in \Omega^{MG}, \ \forall t \in \Omega^T \\ 0 & \forall m \notin \Omega^{B*}, \ \forall k \in \Omega^{MG}, \ \forall t \in \Omega^T \end{cases} \tag{37}$$

In (33)-(37), $\theta_{mn,k,t}^L$ shows the fictitious current flow of distribution lines, $\theta_{m,k,t}^M$ shows the fictitious current flow of the utility grid and $\theta_{m,k,t}^D$ shows the fictitious current flow demand. Constraints (33)-(37) guarantee the radiality of the network. Note that these constraints define a set of fictitious current flows (denoted by θ) in order to energize loads on buses with the possibility of connecting (or reconnecting) to the microgrid. It is clear that any bus m'out of the set $\Omega^{B*}(m' \notin \Omega^{B*})$ has to be in islanded mode and may later be restored by its own DG or battery (if applicable) or mobile MERs, according to the problem situation, which includes transportation road status, available capacity and objective function preferences.

While the above formulation is highly capable of modeling the first stage of the proposed problem, it creates a non-convex MINLP problem, which not only is very difficult to solve, but also does not ensure achieving the optimal solution. In order to overcome this issue, the above formulation needs to be linearized.

D. LINEARIZATION OF THE DISTRIBUTION NETWORK MODEL

The main nonlinearity terms in the formulation of the last section are constraints (21)-(24). In order to linearize these equations, the following new variables need to be defined:

$$f_{mn,k,t}^L = \left(I_{mn,k,t}^L\right)^2 \quad \forall k \in \Omega^{MG}, \forall mn \in \left(\Omega^{DL} \cup \Omega^{TL}\right), \ \forall t \in \Omega^T \tag{38}$$

$$u_{m,k,t} = \left(V_{m,k,t}\right)^2 \quad \forall k \in \Omega^{MG}, \forall m \in \Omega_k^B, \forall t \in \Omega^T \tag{39}$$

By considering the newly defined variables, Eqs. (20)-(26) are respectively updated as follows:

$$\sum_{lm \in \Omega^L} \left[P_{lm,k,t}^L - R_{lm,k} f_{lm,k,t}^L\right] - \sum_{mn \in \Omega^L} P_{mn,k,t}^L + P_{m,k,t}^G + P_{n,k,t}^{MER} - P_{m,k,t}^{Ch} + P_{m,k,t}^{Disch} + \sum_{l \in \Omega^{MG}} P_{l,k,t}^M = P_{m,k,t}^D \ \forall k \in \Omega^{MG}, \ \forall m \in \Omega_k^B, \ \forall n \in \Omega^{MER}, \ \forall t \in \Omega^T \tag{40}$$

$$\sum_{lm \in \Omega^L} \left[Q_{lm,k,t}^L - X_{lm,k} f_{lm,k,t}^L\right] - \sum_{mn \in \Omega^L} Q_{mn,k,t}^L + Q_{m,k,t}^G + Q_{n,k,t}^{MER} + \sum_{l \in \Omega^{MG}} Q_{l,k,t}^M = Q_{m,k,t}^D \quad \forall k \in \Omega^{MG}, \quad \forall m \in \Omega_k^B, \ \forall n \in \Omega^{MER}, \ \forall t \in \Omega^T \tag{41}$$

$$u_{m,k,t} - u_{n,k,t} = 2\left(R_{mn,k} P_{mn,k,t}^L + X_{mn,k} Q_{mn,k,t}^L\right) - \left(Z_{mn,k}\right)^2 f_{mn,k,t}^L + \Delta V_{mn,k,t} \quad \forall mn \in \left(\Omega^{DL} \cup \Omega^{TL}\right), \ \forall k \in \Omega^{MG}, \ \forall t \in \Omega^T \tag{42}$$

$$u_{m,k,t} f_{mn,k,t}^L = \left(P_{mn,k,t}^L\right)^2 + \left(Q_{mn,k,t}^L\right)^2 \quad \forall mn \in \left(\Omega^{DL} \cup \Omega^{TL}\right), \ \forall k \in \Omega^{MG}, \quad \forall t \in \Omega^T \tag{43}$$

$$\left(\underline{V}\right)^2 \le u_{m,k,t} \le \left(\overline{V}\right)^2 \quad \forall k \in \Omega^{MG}, \ \forall m \in \Omega_k^B, \ \forall t \in \Omega^T \tag{44}$$

$$0 \le f_{mn,k,t}^L \le \left(\overline{I^L}\right)^2 w_{mn,k,t}^L \quad \forall k \in \Omega^{MG}, \ \forall mn \in \Omega^{DL}, \ \forall t \in \Omega^T \tag{45}$$

$$0 \le f_{mn,k,t}^L \le \left(\overline{I^L}\right)^2 \quad \forall k \in \Omega^{MG}, \ \forall mn \in \Omega^{TL}, \ \forall t \in \Omega^T \tag{46}$$

$$\left|\Delta V_{mn,k,t}\right| \leq \left[\left(\overline{V}\right)^2 - \left(\underline{V}\right)^2\right]\left(1 - w^L_{mn,k,t}\right) \quad \forall mn \in \left(\Omega^{DL} \cup \Omega^{TL}\right), \quad \forall k \in \Omega^{MG}, \ \forall t \in \Omega^T \tag{47}$$

According to the above new formulation, the newly defined variables can linearize Eqs. (21)-(24). The only remaining nonlinear constraint is (43), which also needs to be linearized, as will be described in the rest of this section.

The left-hand side of (43) can be expressed as follows:

$$u_{m,k,t} f^L_{mn,k,t} = \left[\left(u_{m,k,t} + f^L_{mn,t}\right)/2\right]^2 - \left[\left(u_{m,k,t} - f^L_{mn,t}\right)/2\right]^2 \tag{48}$$

Accordingly, (43) can be rewritten as (49) (we omit k as the MG index from here on out to preserve the simplicity in the shape of our formulation):

$$\left(\omega^+_{mn,t}\right)^2 - \left(\omega^-_{mn,t}\right)^2 = \left(P^L_{mn,t}\right)^2 + \left(Q^L_{mn,t}\right)^2 \quad \forall mn \in \left(\Omega^{DL} \cup \Omega^{TL}\right), \forall t \in \Omega^T \tag{49}$$

where the variables $\omega^+_{mn,t}$ and $\omega^-_{mn,t}$ are defined as:

$$\omega^+_{mn,t} = \left(u_{i,m,t} + f^L_{mn,t}\right)/2, \quad \omega^-_{mn,t} = \left(u_{i,m,t} - f^L_{mn,t}\right)/2 \tag{50}$$

Now, (49) can be linearized using a piecewise-based linearization method:

$$\sum\nolimits_{\lambda=1}^{\Lambda}\left(a^{\omega+}_{\lambda}\delta^{\omega+}_{mn,t,\lambda} + b^{\omega+}_{\lambda}\Delta^{\omega+}_{mn,t,\lambda}\right) - \sum\nolimits_{\lambda=1}^{\Lambda}\left(a^{\omega-}_{\lambda}\delta^{\omega-}_{mn,t,\lambda} + b^{\omega-}_{\lambda}\Delta^{\omega-}_{mn,t,\lambda}\right) = \sum\nolimits_{\lambda=1}^{\Lambda}\left(a^{PL}_{\lambda}\delta^{PL}_{mn,t,\lambda} + b^{PL}_{\lambda}\Delta^{PL}_{mn,t,\lambda}\right) + \sum\nolimits_{\lambda=1}^{\Lambda}\left(a^{QL}_{\lambda}\delta^{QL}_{mn,t,\lambda} + b^{QL}_{\lambda}\Delta^{QL}_{mn,t,\lambda}\right) \quad \forall mn \in \left(\Omega^{DL} \cup \Omega^{TL}\right), \forall t \in \Omega^T \tag{51}$$

$$\omega^+_{mn,t} = \sum\nolimits_{\lambda=1}^{\Lambda}\delta^{\omega+}_{mn,t,\lambda}, \quad \omega^-_{mn,t} = \sum\nolimits_{\lambda=1}^{\Lambda}\delta^{\omega-}_{mn,t,\lambda} \tag{52}$$

$$P^L_{mn,t} = \sum\nolimits_{\lambda=1}^{\Lambda}\delta^{PL}_{mn,t,\lambda}, \quad Q^L_{mn,t} = \sum\nolimits_{\lambda=1}^{\Lambda}\delta^{QL}_{mn,t,\lambda} \tag{53}$$

$$\psi^{PL}_{\lambda-1}\Delta^{PL}_{mn,t,\lambda} \leq \delta^{PL}_{mn,t,\lambda} \leq \psi^{PL}_{\lambda}\Delta^{PL}_{mn,t,\lambda} \tag{54}$$

$$\psi^{QL}_{\lambda-1}\Delta^{QL}_{mn,t,\lambda} \leq \delta^{QL}_{mn,t,\lambda} \leq \psi^{QL}_{\lambda}\Delta^{QL}_{mn,t,\lambda} \tag{55}$$

$$\psi^{PL}_{\lambda-1}\Delta^{PL}_{mn,t,\lambda} \leq \delta^{PL}_{mn,t,\lambda} \leq \psi^{PL}_{\lambda}\Delta^{PL}_{mn,t,\lambda} \tag{56}$$

$$\psi^{QL}_{\lambda-1}\Delta^{QL}_{mn,t,\lambda} \leq \delta^{QL}_{mn,t,\lambda} \leq \psi^{QL}_{\lambda}\Delta^{QL}_{mn,t,\lambda} \tag{57}$$

$$\sum\nolimits_{\lambda=1}^{\Lambda}\Delta^{\omega+}_{mn,t,\lambda} \leq 1, \quad \sum\nolimits_{\lambda=1}^{\Lambda}\Delta^{\omega-}_{mn,t,\lambda} \leq 1 \tag{58}$$

$$\sum\nolimits_{\lambda=1}^{\Lambda}\Delta^{PL}_{mn,t,\lambda} \leq 1, \quad \sum\nolimits_{\lambda=1}^{\Lambda}\Delta^{QL}_{mn,t,\lambda} \leq 1 \tag{59}$$

It is worth mentioning that the superscripts "$\omega+$", "$\omega-$", "PL", and "QL" represent the elements related to the quadratic terms $\left(\omega^+_{mn,t}\right)^2$, $\left(\omega^-_{mn,t}\right)^2$, $\left(P^L_{mn,t}\right)^2$, and $\left(Q^L_{mn,t}\right)^2$, respectively. Also, $\delta_{mn,t,\lambda} \geq 0$ and $\Delta_{mn,t,\lambda} \in \{0, 1\}$ are continuous and binary auxiliary variables, respectively, necessary for acquiring the piecewise linear expressions of the quadratic terms. The symbols ψ_λ, a_λ, and b_λ are constant parameters that can be evaluated as follows:

$$\psi^{\omega+}_{\lambda} = \underline{\omega^+} + (\lambda)\,(1/\Lambda)\left(\overline{\omega^+} - \underline{\omega^+}\right) \tag{60}$$

$$\underline{\omega^+} = (1/2)\left(\underline{V}\right)^2, \quad \overline{\omega^+} = (1/2)\left[\left(\overline{V}\right)^2 + \left(\overline{I^L}\right)^2\right] \tag{61}$$

$$\psi^{\omega+}_{\lambda} = \underline{\omega^-} + (\lambda)\,(1/\Lambda)\left(\overline{\omega^-} - \underline{\omega^-}\right) \tag{62}$$

$$\underline{\omega^-} = (1/2)\left[\left(\underline{V}\right)^2 - \left(\overline{I^L}\right)^2\right], \quad \overline{\omega^-} = (1/2)\left(\overline{V}\right)^2 \tag{63}$$

$$\psi^{PL}_{\lambda} = \psi^{QL}_{\lambda} = (\lambda)\,(1/\Lambda)\,\overline{V}\overline{I^L} \tag{64}$$

$$a^{\omega+}_{\lambda} = \left[\left(\psi^{\omega+}_{\lambda}\right)^2 - \left(\psi^{\omega+}_{\lambda-1}\right)^2\right]/\left[\psi^{\omega+}_{\lambda} - \psi^{\omega+}_{\lambda-1}\right] \tag{65}$$

$$a^{\omega-}_{\lambda} = \left[\left(\psi^{\omega-}_{\lambda}\right)^2 - \left(\psi^{\omega-}_{\lambda-1}\right)^2\right]/\left[\psi^{\omega-}_{\lambda} - \psi^{\omega-}_{\lambda-1}\right] \tag{66}$$

$$a^{PL}_{\lambda} = a^{QL}_{\lambda} = \left[\left(\psi^{PL}_{\lambda}\right)^2 - \left(\psi^{PL}_{\lambda-1}\right)^2\right]/\left[\psi^{PL}_{\lambda} - \psi^{PL}_{\lambda-1}\right] \tag{67}$$

$$b^{\omega+}_{\lambda} = \left(\psi^{\omega+}_{\lambda}\right)^2 - a^{\omega+}_{\lambda}\psi^{\omega+}_{\lambda} \tag{68}$$

$$b^{\omega-}_{\lambda} = \left(\psi^{\omega-}_{\lambda}\right)^2 - a^{\omega-}_{\lambda}\psi^{\omega-}_{\lambda} \tag{69}$$

$$b^{PL}_{\lambda} = b^{QL}_{\lambda} = \left(\psi^{PL}_{\lambda}\right)^2 - a^{PL}_{\lambda}\psi^{PL}_{\lambda} \tag{70}$$

In order to understand the method of obtaining the linear representation of constraint (56), we consider each quadratic term, $\left(\omega^+_{mn,t}\right)^2$, $\left(\omega^-_{mn,t}\right)^2$, $\left(P^L_{mn,t}\right)^2$ and $\left(Q^L_{mn,t}\right)^2$, as $H(x)$. Through the piecewise linearization approach, $H(x)$ is linearized as follows:

$$H(x) = \sum\nolimits_{\lambda=1}^{\Lambda}\left(a_\lambda\delta_\lambda + b_\lambda\Delta_\lambda\right) \tag{71}$$

$$x = \sum\nolimits_{\lambda=1}^{\Lambda}\delta_\lambda \tag{72}$$

$$\psi_{\lambda-1}\Delta_\lambda \leq \delta_\lambda \leq \psi_\lambda\Delta_\lambda \quad \lambda = 1, \ldots, \Lambda \tag{73}$$

$$\sum\nolimits_{\lambda=1}^{\Lambda}\Delta_\lambda \leq 1 \tag{74}$$

$$\delta_\lambda \geq 0, \ \Delta_\lambda \in \{0, 1\} \ \lambda = 1, \ldots, \Lambda \tag{75}$$

In the above formulation, δ_λ and Δ_λ are continuous and binary auxiliary variables, respectively, used to obtain the piecewise linear representation of $H(x)$. Also, ψ_λ, a_λ, and b_λ are constant parameters, evaluated as follows:

$$\psi_\lambda = \underline{x} + \lambda\left(\frac{1}{\Lambda}\right)\left(\overline{x} - \underline{x}\right) \quad \lambda = 1, \ldots, \Lambda \tag{76}$$

$$a_\lambda = \left[H\left(\psi_\lambda\right) - H\left(\psi_{\lambda-1}\right)\right]/\left[\psi_\lambda - \psi_{\lambda-1}\right] \quad \lambda = 1, \ldots, \Lambda \tag{77}$$

$$b_\lambda = H\left(\psi_\lambda\right) - a_\lambda\psi_\lambda \quad \lambda = 1, \ldots, \Lambda \tag{78}$$

In this notation, $\overline{x}$ and $\underline{x}$ show the upper and lower bounds for the variable x, respectively. Fig. 4 depicts the piecewise linear approximation method for a typical quadratic function.

As can be inferred from Fig. 4, the feasible range of variable x is divided into Λ segments. Then, for each segment λ,

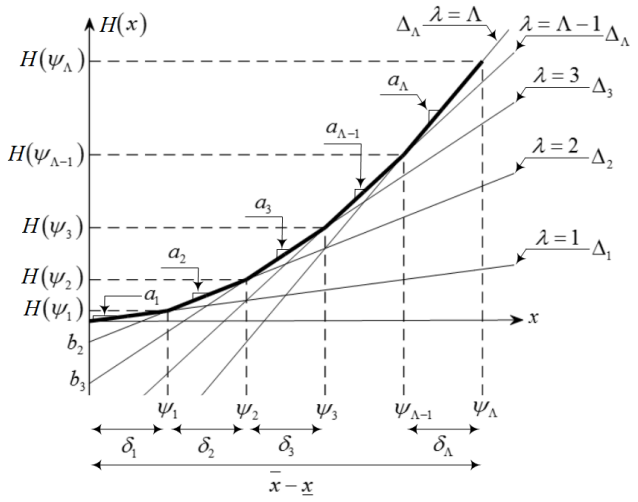

FIGURE 4. Piecewise linear approximation of a typical quadratic function.

a line with a slope of a_λ and intercept of b_λ is considered. Finally, using the binary variable Δ_λ, only one of the lines is chosen to model the nonlinear function $H(x)$. The proposed linear model guarantees obtaining the global optimal solution with a very high accuracy. The high accuracy and performance of the proposed linearization method is demonstrated in the simulation results section. The proposed linearization is quite appropriate for fast and accurate analysis of the microgrids, followed by fast scheduling for units, switches and MERs in a short time.

III. SHORT-PATH ROUTING ALGORITHM

In order to find the optimal routes for delivering MERs to islanded buses or buses with a power shortage, this research uses Dijkstra's algorithm. It is worth noting that there are a number of other path-finding algorithms, such as A* and dynamic programming, which can be used in the same way. Dijkstra's algorithm is capable of solving the one-to-all shortest path problem, which is the problem of determining the shortest path from a candidate node s to all the other nodes in a network, given a weighted network $(\Omega^{\mathbf{S}}, \Omega^{\mathbf{TE}}, \Omega^{\Delta})$ with node set $\Omega^{\mathbf{S}}$, edge set $\Omega^{\mathbf{TE}}$, and weight set Ω^{Δ}, specifying weights c_{ij} for edges $(i, j) \in \Omega^{\mathrm{TE}}$. As has already been mentioned, satellite big data provided before a hurricane will help MERs move to the most appropriate places close enough to the hurricane path for fast delivery to the damaged areas. Therefore, the starting point $s \in \Omega^{\mathrm{S}}$ is known in the post-hurricane management problem. The appropriate destination nodes are determined in stage I of the optimization framework, as described in the last section. In the first stage, the proposed linear power flow determines the healthy buses that have to remain islanded due to the lack of access to any in-service feeder. Depending on the severity of the damage caused by a hurricane in the area, these buses could be restored after optimal switching and reconfiguration, meaning these buses are considered as potential candidates for load restoration using truck-mounted MERs. Considering the limited number of trucks and the possibly damaged roads—which would otherwise be used to access these buses—in the second step, Dijkstra's algorithm is employed to find the shortest paths through healthy roads. In this situation, it is quite likely that some of the buses cannot be accessed at all, due to far distances or severe road damage. In this way, three criteria are considered for picking the most appropriate islanded buses for restoration by truck-mounted MERs: 1) buses with the shortest path from the trucks' initial location ($T^{CL}_{m,k}$), 2) buses with a higher demand side ($P^{D}_{m,k}$) and 3) buses with higher priority ($W_{m,k}$). It is worth noting that in this work we have considered $W_{m,k} = 1$ as showing equal priority for all buses.

This strategy will clearly restore the islanded buses with the shortest path and highest load demand through the truck-mounted MERs. As mentioned above, it is possible that the number of affected buses that need MERs may be more than the number of truck-mounted MERs available, such that only some of them may be restored based on the shortest-path criterion and their priority. In order to avoid trucks taking obstructed routes, these routes (edges) are omitted from the edge set $\Omega^{\mathbf{TE}}$ in Dijkstra's algorithm. The physical distance between two nodes is assumed to be weight c_{ij} for edge (i, j). Then the following steps are used to find the optimal route for delivering MERs to the islanded buses or buses with a power shortage (italic words show special words):

Step I: Pick a truck with the start point $s \in \Omega^{S}$.

Step II: Initialize the status of nodes.

(1) Give the zero distance value to node s, and label it as *Permanent*. [The state of node s becomes $(0, pe)$.]

(2) Assign to every node a distance value of ∞ and label them as *Temporary*. [The states of other nodes become (∞, te).]

(3) Consider node s as the *current* node.

Step III: In this step, the distance value and *current* node designation are updated. Assign i as the index of the *current* node and then:

(1) Determine the set Ω^{J} of nodes with temporary labels that can be touched from the current node i by a link (i, j). [Update the distance values of these nodes.]

(2) For each node $j \in \Omega^{J}$, the distance value d_j is updated using the below equation:

$$d_j^{new} = \min\{d_j, d_i + c_{ij}\} \tag{79}$$

(3) Verify a node j that has the minimum distance value d_j among all nodes $j \in \Omega^{J}$, and find Ω^{J*} such that:

$$min_{j \in J} d_j = d_{j*} \tag{80}$$

(4) Update the label of node j^* to *permanent* and consider this node as the *current* node.

Step IV: Check the termination criterion. If all nodes that can be reached from node s have been permanently labeled, then finish the algorithm (go to step V). If we cannot get to any temporary labeled node from the current node, then all the temporary labels become permanent and the algorithm finishes (go to step V). Otherwise, return to Step III.

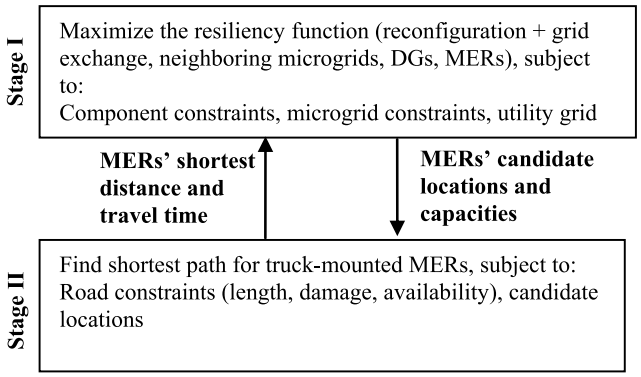

FIGURE 5. Proposed two-stage post-hurricane optimal management framework with reconfiguration and MERs.

Step V: If all the trucks manage to finish the algorithm, end; otherwise return to Step I.

Fig. 5 shows the structure of the proposed two-stage optimization problem. Also, the flowchart of all steps required to run the proposed management framework is provided in Fig. 6.

IV. STOCHASTIC FRAMEWORK BASED ON UT

This section proposes a powerful stochastic framework based on UT [21] to model the uncertainties of the proposed resilient management framework, including the travel time of truck-mounted MERs and active and reactive load values. The proposed stochastic framework is capable of modeling the nonlinear uncertainty in the correlated environment. In comparison with other well-known stochastic methods, such a Monte Carlo simulation, UT can model high uncertainty models with much less computational burden. High uncertainty capturing capability, ease of coding, low computational burden and correlated modeling structure are among the main features of UT. A UT model makes use of the core concept that it is easier to approximate a probability density function than an arbitrary nonlinear function. As a result, it tries to generate fitting samples of input uncertain parameters/variables while preserving their PDF information. In order to better understand this model, let us assume our nonlinear problem as $Y = f(X)$, wherein Y is the output vector, f is the nonlinear function and X is the input random. We also assume that our problem has v uncertain parameters with the mean value μ and covariance P_{xx}. In P_{xx}, the symmetrical component is the uncertain parameter variance and the non-symmetrical components show the covariance between any two uncertain parameters. Having v uncertain parameters, UT attempts to generate $2v+1$ samples and solves the problem $2v+1$ times to handle the uncertainty effects. To this end, the UT model uses the following steps to evaluate the mean μ_y and covariance matrix P_{yy} of the output y:

Step 1: Extract $2v+1$ sample points from the input uncertain data PDF information as follows:

$$X_0 = \mu \tag{81}$$

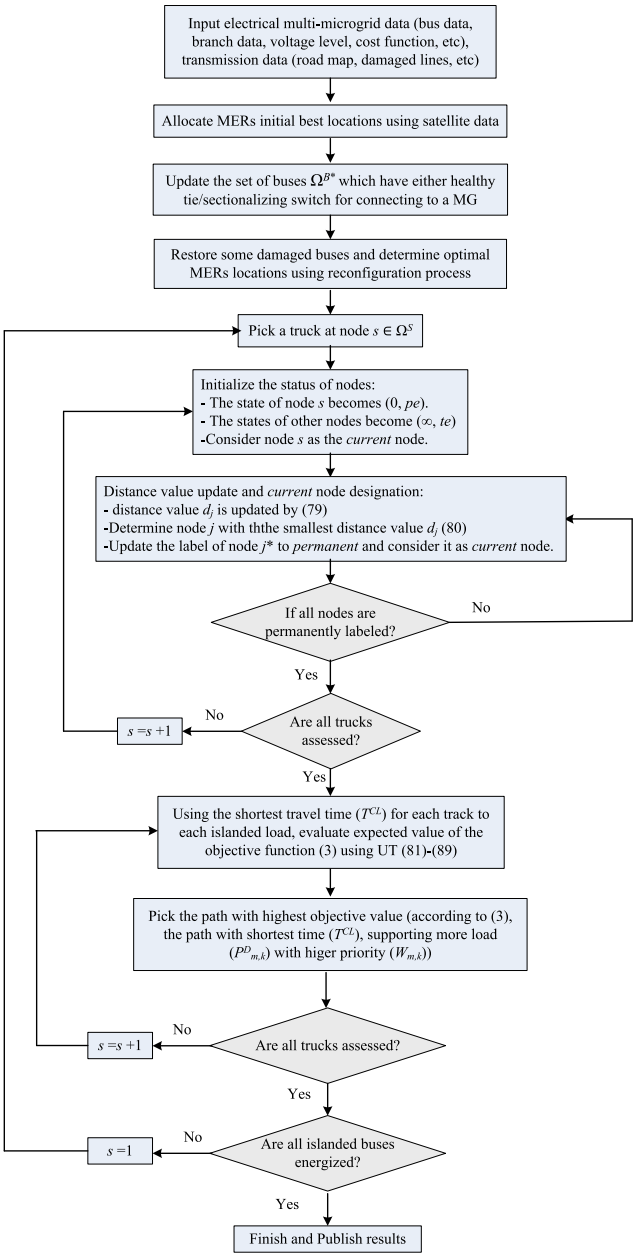

FIGURE 6. Flowchart of the proposed two-stage stochastic post-hurricane optimal management framework with reconfiguration and MERs.

$$X_u = \mu + \left(\sqrt{\frac{v}{1-\beta_0}P_{xx}}\right)_u \quad u = 1, 2, \ldots, v \tag{82}$$

$$X_u = \mu - \left(\sqrt{\frac{v}{1-\beta_0}P_{xx}}\right)_u \quad u = 1, 2, \ldots, v \tag{83}$$

Note that the term $(A)_u$ refers to the u^{th} row or column of matrix A. Also, β_0 is the weight of the mean value μ determined by the operator.

Step 2: Compute the weighting factor for each sample as follows:

$$\beta_0 = \beta_0 \tag{84}$$

$$\beta_u = {(1-\beta_0)}/{2v} \quad u = 1, 2, \ldots, 2v \tag{85}$$

In order to maintain the problem dimension, the summation of the weighting factors should be in unity:

$$\sum_{u\in\Omega^u}^{\beta_u} = 1 \tag{86}$$

Step 3: Feed the $2v + 1$ sample points into the nonlinear function f to find the output samples as follows:

$$Y_u = f(X_u) \tag{87}$$

Step 4: Compute the mean μy and covariance P_{yy} of the output variable Y using the results from step 3 as follows:

$$\mu y = \sum_{u\in\Omega^u}^{\beta_u Y_u} \tag{88}$$

$$P_{yy} = \sum_{u\in\Omega^u}^{\beta_u(Y_u-\mu y)(Y_u-\mu y)^T} \tag{89}$$

Therefore, each time the objective function (3) needs to be evaluated, the above explained stochastic framework is used to find the *expected* value of the objective function, providing more reliable and trustworthy results that show the realistic uncertainty effects of the problem.

V. NUMERICAL SIMULATIONS

A multi-microgrid test system with four interconnected microgrids is considered for studying the performance of the proposed resilient framework. The multi-microgrid system, borrowed from [27], has a total of 68 sectionalizing switches and 4 tie switches (one tie switch inside each microgrid), as shown in Fig. 7. Tie switches 69-73 are located between buses 11-43, 13-21, 15-46, 50-59 and 27-65, respectively. The red dotted lines in this figure show the connecting points of the microgrids. Table 1 shows the characteristics of the DGs in each microgrid. Simulations are implemented in GAMS (first stage) and MATLAB software (second stage) in conjunction with each other. In the stochastic framework, Gaussian distribution PDFs are assumed to model the uncertainty effects with the mean value as the forecast data and a standard deviation of 10% and 7% of base values for truck-mounted MER travel time and active/reactive load demand, respectively. The total CPU time is 1.7 seconds.

Geographic information for an optimal routing comprised of 154 nodes and 269 edges is extracted from [28], as shown

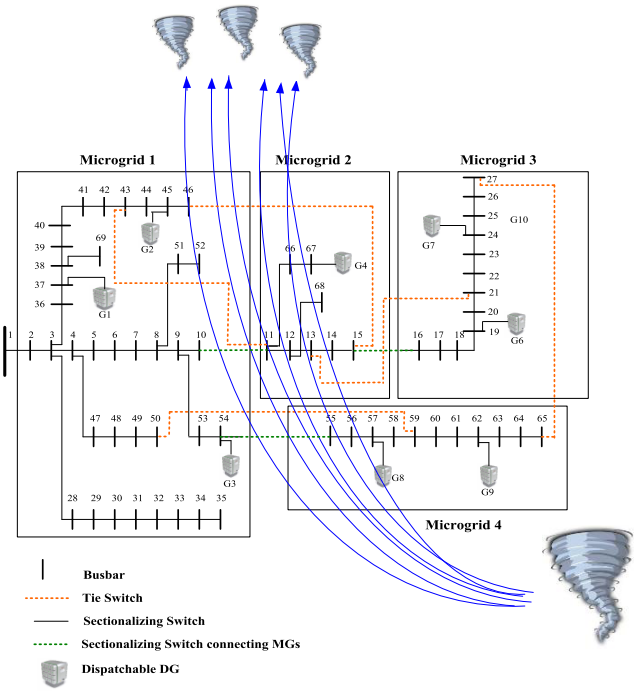

FIGURE 7. One-line diagram of the multi-microgrid test system with a hurricane passing through it [27].

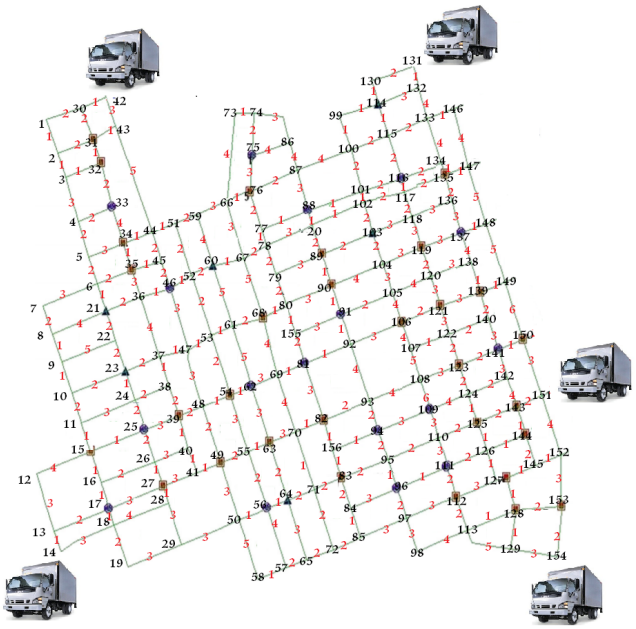

FIGURE 8. Transportation road map and network topology (One distance unit = 2.6 miles).

TABLE 1. Characteristics of DGs

	Unit	Cost Coefficient ($/kWh)	Min-Max Capacity (kW)	Min Up/Down Time (h)	Ramp Up/ Down Rate (kW/h)
	G1	0.154	800-3000	3	1500
	G2	0.167	500-3500	2	1500
	G3	0.167	200-1500	2	1000
microgrid 2	G4	0.157	800-2000	3	1500
	G6	0.208	500-2500	3	1000
	G7	0.195	700-3500	2	1500
	G8	0.167	700-3000	3	1500
	G9	0.184	500-2500	3	1000

in Fig. 8. The nodes are shown using black numbers and route distances are shown using red numbers. It is assumed that the hurricane passes through almost the middle of the networked microgrid, damaging part of the network, as shown in Fig. 7. Information regarding the damaged lines and islanded buses is given in Table 2. Among the damaged lines, two tie

TABLE 2. Information on damaged roads and power lines.

Damaged Lines	Islanded Buses	Out of Order Roads
9-10,10-11, 11-12, **11-43**,12-13, 13-14, 11-66, 66-67, **50-59**, 51-52, 54-55, 55-56	10,11,12,13,52,55,56, 66, 67,68	14, 25, 33, 38, 42, 48,53

TABLE 3. Characteristics of available trucks.

n	$\underline{P_n^{MER}}$ / $\overline{P_n^{MER}}$	$\underline{Q_n^{MER}}$ / $\overline{Q_n^{MER}}$	Parking Location Before Hurricane
1	0/200	0/100	14
2	0/200	0/200	42
3	0/200	0/250	131
4	0/200	0/200	151
5	0/250	0/250	154

switches (normally open) are also affected, which cannot be used in the reconfiguration (shown in bold font in Table 2). The utility has four truck-mounted MERs, each of which is pre-located before the hurricane at the appropriate locations, as listed in Table 3. As mentioned before, based on the prediction methods and distribution system crew experiences, the length of the outage time T^0 is estimated after the hurricane. Normal utility power activities are resumed for serving the loads after T^0. In this study, T^0 is assumed to be 5 hours. Any activity for improving system resilience should be implemented within this time range after the hurricane. It is clear that T^0 can change according to the weather disaster case, ranging from 1 hour to more than a day. Accurate estimation of T^0 is out of the scope of this paper and requires accurate machine learning techniques. Nevertheless, we provide some explanations on T^0 to make the way clear for estimation researchers in the power system. After the accurate estimation of T^0, if the actual outage duration is longer than the estimated duration, the restored loads may face an outage again due to the exhaustion of the MERs. If the actual value of T^0 is smaller than the estimated value, the MER allocation scheme obtained by the proposed framework may be conservative. In this situation and to prevent the restored loads from experiencing an outage again, a larger estimated T^0 is preferable.

In order to clearly show the performance of the proposed resilient framework, the following four cases are studied:

- *Case 0:* Validate the proposed distribution network power flow model in the deterministic framework (ignore uncertainty effects).
- *Case 1:* Ignore reconfiguration and MERs. In this case, no restoration activity is implemented and the system experiences normal utility crew power activities after $t_r + T^O$.
- *Case 2:* Optimal switching is used to restore maximum loads and increase system resilience. Here, MERs are still ignored.
- *Case 3:* Optimal switching and power delivery by MERs are considered to maximize the restored loads. Optimal routing for finding the shortest path is necessary in this case.

It is worth noting that cases 1-3 are simulated in the stochastic framework. In order to verify the accuracy level of the proposed linear power flow model, first we run the power flow on the test system, ignoring all DGs and assuming fixed load values (the original IEEE standard test system). In this way, power losses and bus voltages (magnitude and angle) are evaluated using the proposed linear power flow and compared with those of the well-known recursive backward-forward sweep method. To provide a better comparison, four different load levels, ranging from 50% to 200%, are considered. The accuracy of the proposed power flow model in terms of power losses, bus voltage magnitude and angle error are evaluated as follows:

$$\varepsilon_m^{Ploss} = \left\| \frac{Ploss_m - Ploss_m^{LPF}}{Ploss_m} \times 100 \right\| \quad (90)$$

$$\varepsilon_m^{v} = \left\| \frac{V_m - V_m^{LPF}}{V_m} \times 100 \right\| \quad (91)$$

$$\varepsilon_m^{\theta} = \left\| \frac{\theta_m - \theta_m^{LPF}}{\theta_m} \times 100 \right\| \quad (92)$$

where $Ploss_m$ and V_m/θ_m show the power losses and bus voltage magnitude/angle level calculated by the conventional backward-forward sweep method and $Ploss_m^{LPF}$ and V_m^{LPF}/θ_m^{LPF} show the output of the proposed linear PF. Table 4 shows the simulation results for the network voltage magnitude and angle value for different load levels. It should be mentioned that the abbreviations Avg. and Max. represent the average and maximum of the calculated errors, respectively. According to these results, the proposed linear power flow has provided very highly similar results to those produced using the backward-forward sweep method as a benchmark. These great results are obtained thanks to the high accuracy and performance of the proposed linearization method. In addition, it is seen that increasing the load level increases the voltage error slightly, but again, this increase is small enough to not affect the high accuracy of the method, even for the 200% load level.

TABLE 4. Comparison of voltage magnitudes/angles for different load levels.

Load Levels (%)		50	100	150	200
	Avg.	3×10^{-4}	4×10^{-4}	5×10^{-4}	8×10^{-4}
	Max	0.002	0.003	0.006	0.007
	Avg.	0.007	0.008	0.008	0.009
	Max.	0.013	0.019	0.034	0.041

Table 5 shows the amounts of total power losses for different load levels using the proposed power flow and backward-forward sweep method. As additional evidence, these results show high performance and very low error

TABLE 5. Comparison of total power losses for different load levels.

Load Levels (%)		50	100	150	200
Power Losses (kW)	Backward-Forward Sweep	51.103	222.807	555.051	1119.199
	Proposed Linear PF	51.186	223.041	555.219	1119.389
	Percentage Error (%)	0.1624	0.1050	0.0303	0.0170

values—almost negligible and thus appropriate for any power system study. These results clearly show that the performance of the proposed method does not depend on the size and load values, revealing the high resilience and applicability of the proposed linear power flow.

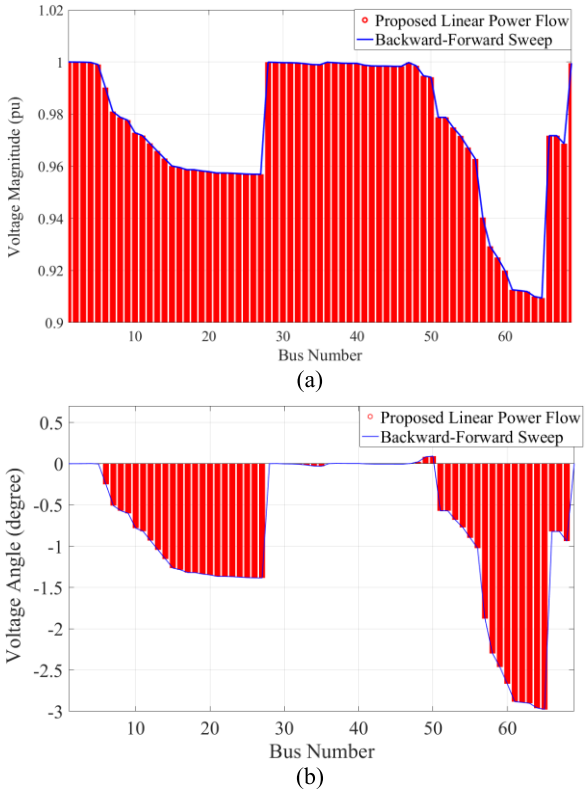

FIGURE 9. Comparison of (a) bus voltage magnitude and (b) bus voltage angle using the proposed linear power flow as well as the backward-forward sweep method for the IEEE test system.

Finally, Fig. 9 shows the comparative plot of the bus voltage magnitude and angle for the peak load (100% load value) using the proposed model and backward-forward sweep method. As shown by our other results, these results also demonstrate the high accuracy of the proposed linearization method, making the model quite suitable for further use in our case.

Table 6 shows the comparative results of islanded buses, total energy not supplied and the resilience objective function. According to these results, optimal reconfiguration could restore loads on buses 14, 15 and 56. Considering instant restoration of the loads through switching, total energy not supplied is reduced by about 649 kWh. The remaining damaged buses, which could not be restored through the reconfiguration, are among the candidates for power delivery by MERs. From a reconfiguration point of view, only tie switch 13-21 remains open; the other two tie switches, 15-46 and 27-65, are in service. By switching (tie switch 27-65) and considering that microgrid four is disconnected from microgrid one after the hurricane, microgrid four can be replaced by microgrid one to support part of its loads. Also, by using tie switch 15-46, the two affected buses, 14 and 15, in microgrid two are energized through bus 46 in microgrid one. These results demonstrate the highly significant performance of the reconfiguration.

TABLE 6. Information on damaged roads and power lines.

Case	Buses without Power Supply	Total Expected Energy Not Supplied (kWh)	Expected Resilience Objective Function
Case 1	10, 11, 12, 13, 14, 15, 52, 55, 56, 66, 68	10,446.847	209,186.11
Case 2	10, 11, 12, 13, 52, 55, 66, 68	9,795.221	211,424.78
Case 3	11, 12, 13	6,084.073	250,725.48

In case 3, five trucks should be scheduled to deliver MERs to the above buses following the shortest-path rule. Please note that buses 10, 11, 12, 13, 52, 55, 66 and 68 are located on physical transportation nodes 54, 69, 92, 56, 67, 83, 89 and 104, respectively. Dijkstra's algorithm will find the shortest path from any departure node s to all candidate buses. Table 7 shows the shortest path simulation results. Each truck starts from the pre-located departure point and passes the nodes shown in Table 7 to get to the islanded bus. Considering one minute for driving one mile, truck-mounted MERs in case 3 could restore buses 10, 52, 55, 66 and 68 in the short time of around half an hour. This increases the resilience objective function and reduces the total energy not supplied, as shown in Table 6. Therefore, only buses 11, 12 and 13 remain without power, which can be arranged during a later power delivery if more MERs become available.

TABLE 7. Optimal routing results for truck-mounted MERs.

Truck Number	Optimal Routes									Distance (mile)
1	14	13	17	16	15	25	39	48	54	31.2
2	42	43	44	45	46	52	60	67		41.6
3	131	130	114	99	100	101	88	20	89	28.6
4	150	141	123	122	104					31.2
5	154	153	128	127	126	111	96	95	83	31.2

In the simulation results of case 3, all roads were assumed to be in service. In order to see the effect of road damage on the resilience function, Table 8 shows the simulation results for different scenarios. Scenario 1 simulates case 3, in which all roads are in service. In the second scenario, since road 25-39 is damaged, truck number one has to drive 2.6 miles more to deliver the MER to bus 10. This has increased

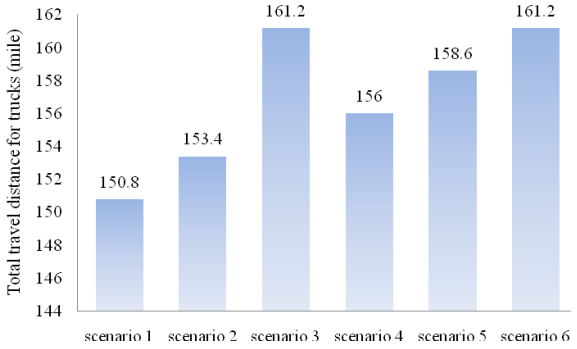

FIGURE 10. Total travel distance for trucks (miles).

TABLE 8. Effect of damaged roads on the restoration process.

Scenario Number	Damaged Roads	Total Expected Energy Not Supplied (kWh)	Expected Resilience Objective Function
1	-	6,084.073	250,725.48
2	25-39	6,083.843	220,512.59
3	45-46,48-54	6,093.209	220,495.56
4	99-100, 123-122	6,072.397	220,502.02
5	130-114,122-123,111-96	6,066.443	220,481.89
6	127-126,95-96, 15-25	6,079.933	220,469.18

the total energy not supplied and devastated the resilience objective function. According to these results, increasing the trucks' travel time will increase the total energy not supplied and reduce network resilience. Nevertheless, this impact is not the same for all trucks. Fig. 10 shows the total travel distance for all trucks. For instance, trucks in scenarios 3 and 6 experience the same driving time, but the system resilience and energy not supplied differ. This is due to the different amount of load supplied by different trucks and MERs.

All cases investigated above are implemented in the first step. Now let us examine a case in which the repair crew is able to fix some components, such as power lines or sectionalizing switches, in the first few hours after a hurricane. Although this case is uncommon, considering the very complicated situation and highly severe damage after a typical hurricane, it can be considered as a possible case (called *Case* 4 here) for some areas that are less affected by a hurricane. Let us assume that tie switch 50-59 is repaired by the repair crew after an hour, and power line 55-56 is repaired at the same time. By energizing line 55-56, bus number 55 is supplied by MG 4 through tie switch 27-65, which was closed in *Case* 3 due to the reconfiguration process. Therefore, there is no need for a MER at bus 55 anymore, meaning it can be used for transferring power to another islanded bus instead. According to the recent simulation results in *Case* 3, buses 11, 12 and 13 are among the best candidates for sending a truck mounted MER to from the starting location of bus 55. Nevertheless, we need to first run the optimal reconfiguration once more to make sure that the network is operating at its optimal structure. Considering the in-service status of tie switch 50-59, the reconfiguration strategy tries to connect MG 4 to MG 1 and simultaneously disconnect it from MG 3. This task can be performed by opening tie switch 27-65 (which was closed in the last step) and closing tie switch 50-59. Through this network reconfiguration process, not only is bus 55 energized by MG 1, but the network power loss is reduced in both MGs 1 and 3. In addition, one MER remains unused and can be sent to any of buses 11, 12 or 13 based on the shortest traveling time ($T^{CL}_{m,k}$), load priority ($W_{m,k}$) and total load demand ($P^{D}_{m,k}$), all of which are incorporated in the objective function (3). Considering the same road condition as in scenario 6 in Table 8, bus 12 is selected by the algorithm as the best candidate. The simulation results in Table 9 clearly show notable improvement in the objective function value and mitigation of the total energy not supplied index."

TABLE 9. Comparative results of *Case* 3 and *Case* 4.

Item	Damaged Roads	Buses without Power Supply	Total Expected Energy Not Supplied (kWh)	Expected Resilience Objective Function
Case 3	127-126,95-96, 15-25	11,12,13	6,079.933	220,469.18
Case 4	127-126,95-96, 15-25	13	5,910.34	220,663.07

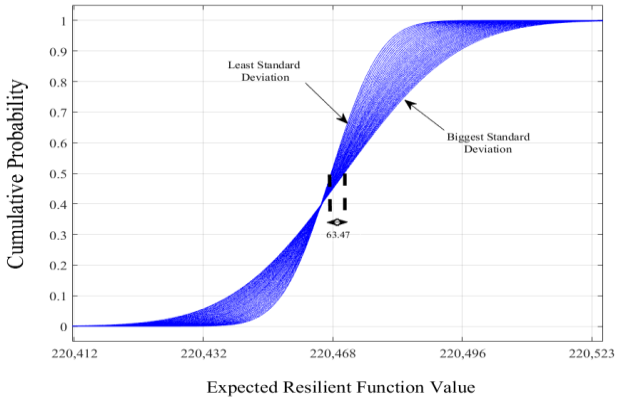

FIGURE 11. Sensitivity Analysis of the Standard Deviation Value of the Uncertain Parameters on the Resilient Function Value.

So far, all simulations were implemented in the stochastic framework and thus provided expected values as the objective functions. This factor is important, since ignoring the uncertainty effects can bring about idealistic results, keeping the operator far from the system's actual operating point in the real world. In order to better perceive the uncertainty effects of the problem, Fig. 11 is provided for *Case* 3, scenario 6. As mentioned before, this paper considers Gaussian PDF with a mean value of the base case to model uncertainty effects. In order to better reveal the effects of uncertainty on the problem, the standard deviation values of all uncertain parameters are changed together and the stochastic framework is run for each case, individually. To this end, the standard deviation values are changed from 0.5 to 4 times their initial value using the discrete step of 0.1. It is clear that

a very low value of standard deviation represents the deterministic framework, while a high standard deviation value shows a system with high uncertainty injections. According to Fig. 11, increasing the standard deviation values of uncertain parameters increases the standard deviation of the resilient objective function, as one would assume. This has resulted in an increase of 63.47 in the expected value of the resilient objective function, meaning that when we consider the uncertainty effects of UT, even with small standard deviation values, much of the uncertainty is modeled already, and increasing the standard deviation value causes only a small increase in the expected value of the resilient objective function.

VI. CONCLUSION

This paper proposed a stochastic two-stage post-hurricane recovery framework for maximizing networked microgrid resilience, incorporating both electrical and transportation constraints. The performance of the proposed method was examined on a practical test system through three different case studies. According to the simulation results, the proposed framework in the first stage could effectively recover parts of the loads by optimal switching. In addition, the first stage determined the potential buses for emergency power delivery, and truck-mounted MERs were sent to the islanded buses based on the optimal routing algorithm. The resilience objective function differs due to the travel time of the trucks carrying the MERs, which varies according to the number and location of damaged routes. The proposed resilient framework can not only reduce the energy not supplied to consumers, but also reduce the costs resulting from a hurricane. From an uncertainty point of view, the proposed linear stochastic framework based on UT shows high capability in modeling uncertainty effects and creating a more reliable and realistic operating point for the grid. Nevertheless, we would like to mention that the stability analysis of such a system after a hurricane, including the dynamic stability, transient analysis and process of connecting MERs to the buses, needs to be investigated in a separate research work. The authors aim to address the stability challenges of this problem in future research.

REFERENCES

[1] J. Lopez, J. E. Rubio, and C. Alcaraz, "A resilient architecture for the smart grid," *IEEE Trans. Ind. Informat.*, vol. 14, no. 8, pp. 3745–3753, Aug. 2018.

[2] Z. Li, M. Shahidehpour, F. Aminifar, A. Alabdulwahab, and Y. Al-Turki, "Networked microgrids for enhancing the power system resilience," *Proc. IEEE*, vol. 105, no. 7, pp. 1289–1310, Jul. 2017.

[3] NOAA National Centers for Environmental Information. (2016). *U.S. Billion-Dollar Weather and Climate Disasters*. Accessed: Jul. 1, 2018. [Online]. Available: https://www.ncdc.noaa.gov/billions/

[4] W. Zeng, Y. Zhang, and M.-Y. Chow, "Resilient distributed energy management subject to unexpected misbehaving generation units," *IEEE Trans. Ind. Informat.*, vol. 13, no. 1, pp. 208–216, Feb. 2017.

[5] A. Kavousi-Fard, and T. Niknam, M. Fotuhi-Firuzabad, "A novel stochastic framework based on cloud theory and θ-modified bat algorithm to solve the distribution feeder reconfiguration," *IEEE Trans. Smart Grid*, vol. 7, no. 2, pp. 740–750, Mar. 2015.

[6] H. Gao, Y. Chen, S. Mei, S. Huang, and Y. Xu, "Resilience-oriented pre-hurricane resource allocation in distribution systems considering electric buses," *Proc. IEEE*, vol. 105, no. 7, pp. 1214–1233, Jul. 2017.

[7] C. G. Rieger, "Notional examples and benchmark aspects of a resilient control system," in *Proc. 3rd Int. Symp. Resilient Control Syst.*, Idaho Falls, ID, USA, Aug. 2010, pp. 64–71.

[8] M. Rayati and A. M. Ranjbar, "Resilient transactive control for systems with high wind penetration based on cloud computing," *IEEE Trans. Ind. Informat.*, vol. 14, no. 3, pp. 1286–1296, Mar. 2018.

[9] D. Henry and J. E. Ramirez-Marquez, "Generic metrics and quantitative approaches for system resilience as a function of time," *Rel. Eng. Syst. Saf.*, vol. 99, pp. 114–122, Mar. 2012.

[10] D. A. Reed, K. C. Kapur, and R. D. Christie, "Methodology for assessing the resilience of networked infrastructure," *IEEE Syst. J.*, vol. 3, no. 2, pp. 174–180, Jun. 2009.

[11] Y. Wang, C. Chen, J. Wang, and R. Baldick, "Research on resilience of power systems under natural disasters—A review," *IEEE Trans. Power Syst.*, vol. 31, no. 2, pp. 1604–1613, Mar. 2016.

[12] G. Dong and Z. Chen, "Data driven energy management in a home microgrid based on Bayesian optimal algorithm," *IEEE Trans. Ind. Informat.*, to be published.

[13] S. Mohagheghi and F. Yang, "Applications of microgrids in distribution system service restoration," in *Proc. IEEE PES Innov. Smart Grid Technol.*, Anaheim, CA, USA, Jan. 2011, pp. 1–7.

[14] B. Ansari and S. Mohagheghi, "Electric service restoration using microgrids," in *Proc. IEEE PES Gen. Meeting, Nat.*, Harbor, MD, USA, Jul. 2014, pp. 1–5.

[15] C. Chen, J. Wang, F. Qiu, and D. Zhao, "Resilient distribution system by microgrids formation after natural disasters," *IEEE Trans. Smart Grid*, vol. 7, no. 2, pp. 958–966, Mar. 2016.

[16] Z. Wang and J. Wang, "Self-healing resilient distribution systems based on sectionalization into microgrids," *IEEE Trans. Power Syst.*, vol. 30, no. 6, pp. 3139–3149, Nov. 2015.

[17] K. P. Schneider, F. K. Tuffner, M. A. Elizondo, C.-C. Liu, Y. Xu, and D. Ton, "Evaluating the feasibility to use microgrids as a resiliency resource," *IEEE Trans. Smart Grid*, vol. 8, no. 2, pp. 687–696, Mar. 2017.

[18] H. Ahmadi, A. Alsubaie, and J. R. Martí, "Distribution system restoration considering critical infrastructures interdependencies," in *Proc. IEEE PES General Meeting*, National Harbor, MD, USA, Jul. 2014, pp. 1–5.

[19] A. Alsubaie *et al.*, "A platform for disaster response planning with interdependency simulation functionality," in *Proc. 7th Int. Conf. Crit. Infrastruct. Protection (ICCIP)* in IFIP Advances in Information and Communication Technology AICT, vol. 417, J. Butts and S. Shenoi, Eds. Washington, DC, USA: Springer, Mar. 2013, pp. 183–197. [Online]. Available: https://hal.inria.fr/hal-01456885/document

[20] B. Chen, C. Chen, J. Wang, and K. L. Butler-Purry, "Sequential service restoration for unbalanced distribution systems and microgrids," *IEEE Trans. Power Syst.*, vol. 33, no. 2, pp. 1507–1520, Mar. 2017.

[21] A. Kavousi-Fard, and T. Niknam, M. Fotuhi-Firuzabad, "Stochastic reconfiguration and optimal coordination of V2G plug-in electric vehicles considering correlated wind power generation," *IEEE Trans. Sustain. Energy*, vol. 6, no. 3, pp. 822–830, Jul. 2015.

[22] Z. Bie, Y. Lin, G. Li, and F. Li, "Battling the extreme: A study on the power system resilience," *Proc. IEEE*, vol. 105, no. 7, pp. 1253–1266, Jul. 2017.

[23] S. Lei, J. Wang, C. Chen, and Y. Hou, "Mobile emergency generator pre-positioning and real-time allocation for resilient response to natural disasters," *IEEE Trans. Smart Grid*, vol. 9, no. 3, pp. 2030–2041, May 2017.

[24] S. E. Middleton, L. Middleton, and S. Modafferi, "Real-time crisis mapping of natural disasters using social media," *IEEE Intell. Syst.*, vol. 29, no. 2, pp. 1–17, Mar./Apr. 2014.

[25] G. Shi and K. Barker, "Extraction of geospatial information on the Web for GIS applications," in *Proc. 10th IEEE Int. Conf. Cognit. Inform. Cognit. Comput.*, Aug. 2011, pp. 41–48.

[26] B. Tellman, B. Schwarz, R. Burns, and C. Adams. (2015). Big Data in the Disaster Cycle: Overview of use of Big Data and Satellite Imaging in Monitoring Risk and Impact of Disasters. Chapter Disaster Risk Reduction, UN Development. [Online]. Available: https://math.la.asu.edu/~dieter/courses/Graduate_modeling/BigDataSatellitesandDisasterMonitoringFINAL.docx

[27] S. A. Arefifar, M. Ordonez, and Y. A.-R. I. Mohamed, "Energy management in multi-microgrid systems—Development and assessment," *IEEE Trans. Power Sys.*, vol. 32, no. 2, pp. 910–922, Mar. 2017.
[28] S.-H. Huang and P.-C. Lin, "Vehicle routing-scheduling for municipal waste collection system under the 'keep trash off the ground' policy," *Omega*, vol. 55, pp. 24–37, Sep. 2015.

ABDOLLAH KAVOUSI-FARD (M'13) received the B.Sc. degree from the Shiraz University of Technology, Shiraz, Iran, in 2009, the M.Sc. degree from Shiraz University, Shiraz, in 2011, and the Ph.D. degree from the Shiraz University of Technology in 2016, all in electrical engineering. He was a Post-Doctoral Researcher with the University of Michigan-Dearborn, USA, from 2016 to 2018. He was a Researcher with the University of Denver, Denver, CO, USA, from 2015 to 2016. His current research interests include operation, management and cyber security analysis of smart grids, microgrid, smart city, electric vehicles and protection of power systems, reliability, artificial intelligence, and machine learning.

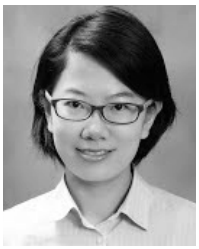

MENGQI WANG (S'11–M'15) received the B.S. degree in electrical engineering from Xi'an Jiaotong University, Xi'an, China, in 2009, and the Ph.D. degree in electrical engineering from North Carolina State University, Raleigh, NC, USA, in 2014. Since 2015, she has been an Assistant Professor with the Department of Electrical and Computer Engineering, University of Michigan-Dearborn, Dearborn, MI, USA. Her research interests include dc–dc and dc–ac power conversions, high efficiency and high-power density power supplies, renewable energy systems, and wide-bandgap power device applications.

WENCONG SU (S'06–M'13–SM'18) received the B.S. degree (Hons.) from Clarkson University, Potsdam, NY, USA, in 2008, the M.S. degree from Virginia Tech, Blacksburg, VA, USA, in 2009, and the Ph.D. degree from North Carolina State University, Raleigh, NC, USA, in 2013, respectively. He is currently an Assistant Professor with the Department of Electrical and Computer Engineering, University of Michigan-Dearborn. His current research interests include power systems, electrified transportation systems, and cyber-physical systems. He is an Editor of the IEEE Transactions on Smart Grid.